

Magnetic Resonance Thermometry of Focused Ultrasound Using a Preclinical Focused Ultrasound Robotic System at 3T

Antria Filippou¹, Nikolas Evripidou¹, Andreas Georgiou¹, Leonidas Georgiou², Antreas Chrysanthou², Cleanthis Ioannides², Christakis Damianou^{1,3}

¹Department of Electrical Engineering, Computer Engineering and Informatics, Cyprus University of Technology, ²Department of Interventional Radiology, German Oncology Centre, Limassol, Cyprus, ³Department of Electronics and Information Engineering, Hangzhou Dianzi University, Hangzhou, China

Abstract

Aim: Focused ultrasound (FUS) therapies are often performed within magnetic resonance imaging (MRI) systems providing thermometry-based temperature monitoring. Herein, MRI thermometry was assessed for FUS sonications executed using a preclinical system on agar-based phantoms at 1.5T and 3T MRI scanners, using the proton resonance frequency shift technique. **Materials and Methods:** Sonications were executed at 1.5T and 3T to assess the system and observe variations in magnetic resonance (MR) thermometry temperature measurements. MR thermometry was assessed at 3T, for identical sonications on three agar-based phantoms doped with varied silica and evaporated milk concentrations, and for sonications executed at varied acoustic power of 1.5–45 W. Moreover, echo time (TE) values of 5–20 ms were used to assess the effect on the signal-to-noise ratio (SNR) and temperature change sensitivity. **Results:** Clearer thermal maps with a 2.5-fold higher temporal resolution were produced for sonications at 3T compared to 1.5T, despite employment of similar thermometry sequences. At 3T, temperature changes between 41°C and 50°C were recorded for the three phantoms produced with varied silica and evaporated milk, with the addition of 2% w/v silica resulting in a 20% increase in temperature change. The lowest acoustic power that produced reliable beam detection within a voxel was 1.5 W. A TE of 10 ms resulted in the highest temperature sensitivity with adequate SNR. **Conclusions:** MR thermometry performed at 3T achieved short temporal resolution with temperature dependencies exhibited with the sonication and imaging parameters. Present data could be used in preclinical MRI-guided FUS feasibility studies to enhance MR thermometry.

Keywords: Agar, magnetic resonance imaging, thermometry, ultrasound

Received on: 31-07-2024

Review completed on: 24-10-2024

Accepted on: 12-11-2024

Published on: 18-12-2024

INTRODUCTION

Since its introduction seven decades ago,^[1] high-intensity focused ultrasound (HIFU) has been extensively explored in almost every human tissue, emerging as a noninvasive clinical surgical tool for a wide range of oncological and nononcological applications.^[2,3] HIFU therapeutic techniques employ ultrasound (US) waves that locally focus within tissue to raise its temperature to hyperthermic or ablative levels,^[2] with the procedures typically guided by US or magnetic resonance imaging (MRI) systems that provide treatment monitoring.^[3] MRI guidance offers superior performance than US-guided systems since it provides increased image spatial resolution^[4] and enables real-time noninvasive quantitative monitoring of the tissue temperature increase through magnetic resonance (MR) thermometry techniques.^[5] MR thermometry is a potent temperature monitoring tool utilizing various temperature dependent methods such as the proton resonance frequency

shift (PRF), proton density, T_1 relaxation time mapping, T_2 relaxation time mapping, apparent diffusion coefficient, and magnetization transfer.^[6]

Among the various techniques, the PRF is considered the gold standard and the only clinically available method for monitoring temperature evolution in MRI-guided FUS (MRgFUS) applications,^[7] since it is aqueous tissue type independent and offers a proportional correlation with temperature over a large temperature range.^[5] The technique is based on the temperature dependence of the hydrogen

Address for correspondence: Dr. Christakis Damianou, Department of Electrical Engineering, Computer Engineering and Informatics, Cyprus University of Technology, 30 Archbishop Kyprianou Street, 3036 Limassol, Cyprus. E-mail: christakis.damianou@cut.ac.cy

This is an open access journal, and articles are distributed under the terms of the Creative Commons Attribution-NonCommercial-ShareAlike 4.0 License, which allows others to remix, tweak, and build upon the work non-commercially, as long as appropriate credit is given and the new creations are licensed under the identical terms.

For reprints contact: WKHLRPMedknow_reprints@wolterskluwer.com

How to cite this article: Filippou A, Evripidou N, Georgiou A, Georgiou L, Chrysanthou A, Ioannides C, *et al.* Magnetic resonance thermometry of focused ultrasound using a preclinical focused ultrasound robotic system at 3T. *J Med Phys* 2024;49:583-96.

Access this article online

Quick Response Code:



Website:
www.jmp.org.in

DOI:
10.4103/jmp.jmp_133_24

bonds that at increased tissue temperatures result in increased electron screening and ultimately decreased PRF.^[5,6] These resonant frequency changes induce a phase shift in MRI images acquired during HIFU treatments, which PRF utilizes to provide HIFU induced temperature changes in the form of thermal mapping, by subtracting the phases of MR images acquired prior and throughout HIFU heating.^[5,6] PRF is usually employed for MR thermometry in MRI scanners with field strengths between 1T^[8] and 3T,^[9] and is typically implemented with Gradient echo (GRE) sequences that provide simple and relatively high temperature sensitivities.^[5] However, more rapid sequences such as Echo planar imaging (EPI), segmented EPI, or single-shot EPI (ss-EPI) can be employed to rapidly generate MR thermometry data,^[8,10,11] albeit with these sequences negatively impacting the quality of acquired images, thus affecting temperature estimations.^[8,12]

Notably, the type of imaging sequence, when used with similar acquisition parameters, does not seem to affect the image signal-to-noise ratio (SNR) in either 1.5T or 3T scanners,^[8] with increased SNR and PRF sensitivity observed at both field strengths at echo times (TE) closer to the T2* relaxation times of the tissue under investigation,^[8,13,14] and for flip angles similar to the Ernst angle.^[14] Moreover, SNR dependencies with the sampling bandwidth have been reported at 3T, with a low bandwidth resulting in high SNR however, with possible presence of off-resonance artifacts.^[15] Recently, multiecho spiral^[15] and multislice^[13] thermometry sequences were reported to result in enhanced and faster MR thermometry with decreased artifacts and better resolution compared to conventional sequences, thus suited for monitoring *in vivo* HIFU sonications at 3T.^[13,15]

Lately, an increased number of MRgFUS studies are performed within a higher field scanner (3T) since the increased magnetic field strength leads to higher temperature sensitivity,^[6] increased measurement accuracy and smaller temperature variations compared to 1.5T scanners.^[8] Although the PRF is considered the preferred method for MR thermometry monitoring in HIFU tissue ablations, the technique has been reported as inferior for monitoring *in vivo* pulsed^[16] or hyperthermic^[17] MRgFUS procedures executed inside 3T MRI scanners since it underestimates temperatures and requires factor^[16] and phase^[17] corrections, respectively, to yield accurate temperatures. However, recently, a graphical interface was developed for real-time PRF MR thermometry for hyperthermic HIFU prostate applications,^[18] with feasibility studies executed in phantoms inside a 3T scanner generating temperature maps with a minimal temperature error (0.5°C).^[18]

Notwithstanding its high accuracy, PRF is sensitive to magnetic field changes and organ motion,^[6] with MRgFUS studies at 3T also demonstrating temperature artifacts and errors arising due to magnetic susceptibility differences induced by injection of MRI contrast agents.^[19] Subsequently, several techniques such as two-step filters,^[20] multibaseline,^[21] or referenceless algorithms^[22-24] have been successfully employed and validated in 3T scanners for compensation of artifacts present.^[20-24]

Nevertheless, in phantom experiments executed in both a 1.5T and 3T scanners, referenceless thermometry has been reported as inferior at 3T for adjusting magnetic field changes.^[24] Notably, *in vivo* studies^[21,23] executed at 3T have shown that respiration induced noise in PRF MR thermometry can be decreased by applying motion compensation multibaseline algorithms^[21] or using rapid segmented interleaved EPI sequences for successfully monitoring HIFU treatments of moving organs.

Moreover, although PRF is preferred because of its aqueous tissue independency,^[25] employment of the technique for temperature monitoring in fat tissues poses significant difficulties^[25] attributed to absence of hydrogen bonds.^[26] In such manner, fat suppression techniques are usually employed^[10,27,28] to account for temperature estimation errors attributed to phase difference modifications related to lipid presence^[25] and magnetic field susceptibilities arising during HIFU fat ablation.^[29,30] Nevertheless, several techniques combining PRF and T1 or T2 mapping have been examined for performing MR thermometry for fat at high field scanners.^[7] Diakite *et al.*^[31] developed a hybrid PRF-T1 mapping sequence to provide concurrent temperature imaging of aqueous and fat tissues in a 3D plane, with feasibility studies executed at 3T on excised tissue providing high SNR temperature maps of aqueous and fat tissues, thus indicating potential clinical applications of the technique.^[31]

As abovementioned, PRF calculates temperature changes by utilizing differences in the phase of the acquired MRI images.^[5,6] Noteworthy, the phase of the images represents a single rotation of the MRI signal, characterized by both amplitude and direction taking values between $-\pi$ and π .^[32] In this regard, signal rotations outside of this 2π range are wrapped around to gain values in the constrained range, thus making the real phase values indistinguishable.^[32] Subsequently, unwrapping algorithms^[33-35] need to be employed on matrix voxels of the acquired wrapped phase images to uncover the correct phase value, thus resulting in accurate estimations of the induced temperature change. Notably, Kim *et al.*^[36] developed a program for generating PRF MR thermometry data, wherein the phase difference is not directly calculated from phase values, but is rather determined by subtracting complex numbers, thus sparing the need for unwrapping algorithms. Accurate temperatures were acquired with the program for HIFU sonications executed *ex vivo* in a 3T scanner for an SPGR sequence.^[36]

Considering the increasing development of novel MRgFUS systems^[37] and the recent improvements in MR thermometry techniques for monitoring temperature evolution during therapeutic procedures,^[7] in this study, the PRF technique was employed for assessing the sensitivity, temporal and spatial resolution of MR thermometry monitoring during HIFU sonications executed on agar-based phantoms doped with silica.^[38-42] HIFU exposures were performed with a preclinical MRgFUS robotic system^[43] with the PRF-based MR thermometry data generated using an inhouse MRgFUS

software with treatment planning and MR thermometry capabilities.^[44] HIFU sonications were executed within two clinical MRI scanners of varied magnetic field strength, namely 1.5T and 3T, to assess the performance of the preclinical MRgFUS robotic system^[43] within the different MRI environments and examine any variations in thermometry mapping arising from the varied magnetic field strength. Moreover, dependencies of the temporal and spatial resolution of MR thermometry temperature measurements with the HIFU sonication parameters and MR sequence acquisition parameters were examined for a series of sonications executed at 3T, evaluating the system and optimizing thermometry sequences at the higher magnetic field scanner.

MATERIALS AND METHODS

Proton resonance frequency magnetic resonance thermometry calculations

MR thermometry data were generated using the widely used PRF technique^[5,6] that relates the temperature changes (ΔT) that influence the precession frequency of protons to the phase shift ($\Delta\phi$) observed in the MRI signal. The phase shift is calculated from the phase of MR images of the tissue under treatment acquired at baseline temperatures before heating and at specific time intervals during HIFU heating. Typically, more than one reference images are acquired at baseline temperatures before heating to account for pulse sequence variability. The temperature change (ΔT) from baseline is then calculated from the cumulative phase difference of the images acquired before and during heating using the following Equation 1:

$$\Delta T = \frac{\varphi(T) - \varphi(T_o)}{\gamma \cdot \alpha \cdot B_o \cdot TE} \quad (1)$$

where $\varphi(T)$ is the phase of the image acquired during heating, $\varphi(T_o)$ is the phase difference of the reference images acquired at baseline temperature, γ is the gyromagnetic ratio, α is the PRF temperature change tissue coefficient, B_o is the local magnetic field strength and TE is the TE of the MR imaging sequence. The PRF temperature change coefficient is a tissue constant taking values in the -0.007 to -0.011 ppm/ $^{\circ}\text{C}$ range.^[6] MR thermometry data presented herein were calculated using a PRF temperature change tissue coefficient of -0.01 ppm/ $^{\circ}\text{C}$. This is considered as the typical PRF coefficient^[6] and a value that is commonly reported for the PRF coefficient of agar-based phantoms.^[45-47]

Magnetic resonance imaging-guided focused ultrasound software with magnetic resonance thermometry monitoring capabilities

An inhouse user friendly MRgFUS software written in the C# (Visual Studio, Microsoft Corporation) language^[47] was implemented for generating PRF-based MR thermometry data. The software controls the motion and sonication parameters of various preclinical MRgFUS robotic systems equipped with single element focused transducers developed for specific applications.^[43,48-53] In a typical experimental setting

within the MRI environment, the software interfaces with the robotic system, and navigates the ultrasonic transducer along predetermined trajectories. Specifically, transducer navigation is performed according to user commands that determine the size of the sonication trajectory (single point or grid operation), the spatial resolution of the transducer's navigation (grid spatial step) as well as the time delay amidst consecutive sonications. Moreover, the sonication parameters of the treatment are appropriately adjusted through user commands relating to the transducer's operating frequency, the applied power as well as the sonication time. The software additionally offers MRI interfacing capabilities, enabling direct acquisition of MR images from clinical MRI scanners, therefore allowing treatment planning and HIFU treatment monitoring using MR thermometry.^[47]

MR thermometry data for HIFU treatments with the software are generated based on the PRF technique. During interfacing with a clinical scanner, two types of MRI images, specifically magnitude and phase images of the subject undergoing MRgFUS sonications, are exported from the MRI scanner to the developed software using a script written in the Python language (Python Software Foundation, Delaware, USA) and a series of Python libraries (Proteus MRI-HIFU Software Development Suite). The flowchart of the PRF-based MR thermometry calculations executed by the software is shown in Figure 1. The software directly retrieves and reads the reference magnitude and phase images of the subject, acquired at baseline temperatures before HIFU heating. The reference magnitude image of the tissue is then displayed by the software on the available graphical user interface (GUI). Notably, the region of interest (ROI) where the focal spot is located, and where ultimately MR thermometry calculations are performed, is automatically generated by the software, and is overlapped as a small red point on the displayed magnitude image of the subject. Nevertheless, the software allows the user to manually adjust the location of the ROI appropriately. Concurrently, the magnitude and phase images of the subject, acquired during the HIFU ablations are retrieved and read by the software using the Python script (Python Software Foundation). Upon retrieval of both the reference and ablation images, the phase difference between the two types of images is calculated, followed by application of certain unwrapping algorithms that adjust for the wrapped around phases and retrieve the actual rotation of the phase signal.^[32] The unwrapped phase differences are followed by application of intrascan transient phase offset correction on the calculated phase difference. Thereafter, the induced temperature shift is calculated in a pixel-by-pixel approach on the defined ROI, using the PRF method and Equation 1. Advantageously, the other three variables (local magnetic field strength, α PRF coefficient, and TE) required for MR thermometry calculations have already been acquired by the software. Specifically, the temperature tissue coefficient α is commanded by the user through the GUI of the software alongside other variables that affect MR thermometry calculations (i.e., baseline temperature of subject



Figure 1: Flowchart of the proton resonance frequency-based magnetic resonance thermometry calculations

and number of reference images acquired). Regarding the TE and magnetic field strength values, these data are automatically acquired by the software from the reference magnitude images of the subject. After the calculations, a color-coded thermal map of the temperature, and a time series temperature graph are demonstrated by the software, therefore enabling PRF-based MR thermometry monitoring of the sonications executed within the corresponding ROI.

Notably, the color-coded thermal map is also overlapped on the equivalent ROI on the magnitude image of the subject, thus permitting visual depiction of the location and extent of thermal heating relative to the spatial anatomy of the subject. Furthermore, the generated MR thermometry data are saved and automatically updated throughout the procedure upon acquisition of new MRI images. In this regard, the time resolution at which MR thermometry data are generated is determined and limited by the temporal resolution of the

MR sequence employed for imaging the HIFU sonications. Figure 2 shows an indicative example of the MR thermometry monitoring provided by the software, with MR thermometry data generated for sonications executed on agar-based phantoms^[38-42] that are habitually employed in MRgFUS studies.^[54] The color-coded thermal map, the thermal map overlapped on the magnitude image of the phantom and the time series tissue temperature graph are calculated and presented on the GUI, next to the treatment planning image, therefore allowing PRF-based MR thermometry monitoring.

Magnetic resonance imaging-guided focused ultrasound robotic system

A previously developed MRgFUS robotic system^[43] was utilized for executing HIFU sonications on agar-based phantoms doped with silica^[38-42] within a clinical MRI environment. The MRI compatible robotic system is integrated with a single element spherically focused transducer that operates within a container

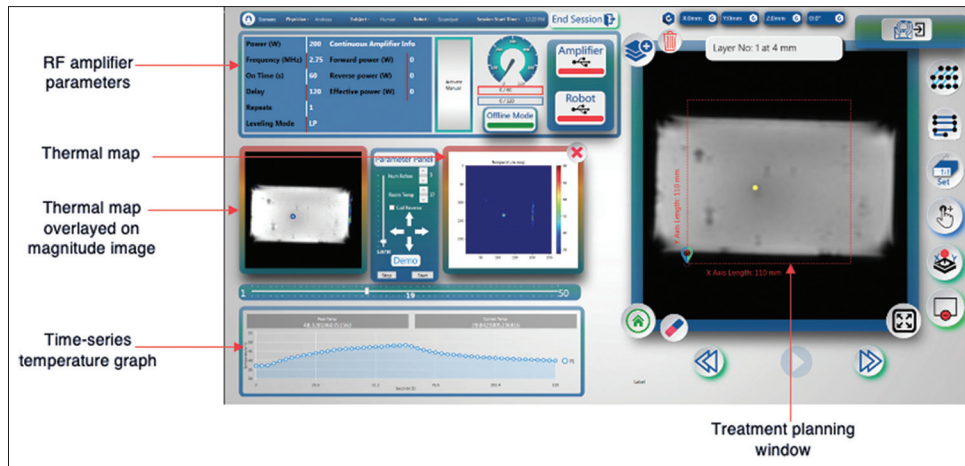


Figure 2: Screenshot of the inhouse software providing magnetic resonance thermometry monitoring

filled with deionized/degassed water and is navigated along three linear stages through computer-controlled motion actuated by piezoelectric motors.^[43] In this study, an inhouse developed ultrasonic transducer operating at a frequency of 2.6 MHz, having a diameter of 50 mm, focusing beam at 65 mm, and having a 30% efficiency was integrated in the robotic system.

The robotic system was placed on the table of either a 1.5T (Signa HDxt 16x, GE Healthcare, Chicago, Illinois, USA) or 3T (Magnetom Vida, Siemens Healthineers, Erlangen, Germany) clinical MRI scanner. The agar-based phantom, developed with appropriate concentrations of inclusion materials, was accommodated on the acoustic opening of the robotic system as indicatively shown in Figure 3 for the 3T scanner (Magnetom Vida, Siemens Healthineers). A 3D printed (F270, Stratasys, Minnesota, USA) Acrylonitrile Styrene Acrylate (ASA) structure was positioned around the robotic system to support the MR coil employed for imaging the executed sonication protocols. The robotic system was connected through cables to an inhouse developed electronic system that controls the motion of the motors, while the transducer was connected to an RF amplifier (AG1016, T and C Power Conversion, Rochester, NY, USA) for powering purposes. It is worth stating that the electronic system, software, and RF amplifier were located within the MRI control room.

Agar-based tissue mimicking materials

Agar-based phantoms were developed and utilized as targets during sonications since they exhibit a high melting point^[54] that can withstand the temperatures normally induced by high intensity sonications. In this study, agar-based phantoms were produced following a preparation procedure mentioned in the literature^[38] and utilizing certain inclusion materials that in specific concentrations can precisely mimic the acoustic and thermal properties of human tissues^[38,40-42] as well as produce a human tissue-like MRI signal.^[39] In this regard, agar (10164, Merck KGaA, Darmstadt, Germany) and silica (Sigma-Aldrich, Missouri, USA) powders, as well as

liquid evaporated milk (Nounou, Friesland Campina, Marousi, Greece) were employed in specific percent (%) weight per volume (w/v) or volume per volume (v/v) concentrations, respectively, following the preparation procedure mentioned by Drakos *et al.*^[38] The tissue mimicking materials were developed in a 3D printed (F270, Stratasys) mold with dimensions 90 mm (w) × 160 mm (l) × 100 mm (h), thus allowing support of the rectangular agar-based phantom on the acoustic window of the robot.

Magnetic resonance thermometry for sonications at 1.5T and 3T

A fast spoiled gradient echo (FSPGR) sequence with the following parameters: Repetition time (TR) = 20 ms, TE = 10 ms, Field of View (FOV) = 28 × 28 cm², Slice thickness = 10 mm, Acquisition Matrix = 128 × 128, Number of Excitations (NEX) = 2, Echo train length (ETL) = 1, and Flip angle = 35°, was employed along with a General Purpose Flex (GPFLEX) surface coil (GPFLEX, Signa 1.5T receiver only, GE Healthcare) for MR imaging the agar-based phantoms during sonications within the 1.5T MRI scanner (Signa HDxt 16x, GE Healthcare; 33 mT/m maximum gradient amplitude, 120 T/m/ms slew rate, 100% duty cycle, 0.02 ppm homogeneity over a 20 cm diametrical spherical volume). Notably, the FSPGR sequence with the abovementioned acquisition parameters induced a specific absorption rate (SAR) of 1.771 W/kg within the agar-based phantoms during MR image acquisition.

Accordingly, MRI scans of the agar-based phantoms during sonications implemented within the 3T scanner (Magnetom Vida, Siemens Healthineers; 45 mT/m maximum gradient amplitude, 200 T/m/ms slew rate, 100% duty cycle, 0.04 ppm homogeneity over a 20 cm diametrical spherical volume) were executed using a fast low angle shot (FLASH) sequence, which is similar to the FSPGR sequence employed for imaging inside the 1.5T MRI scanner (Signa HDxt 16x, GE Healthcare). The agar-based phantoms were imaged using a body coil (Body18, Siemens Healthineers) and the FLASH sequence that was used with comparable acquisition parameters (TR = 20 ms,

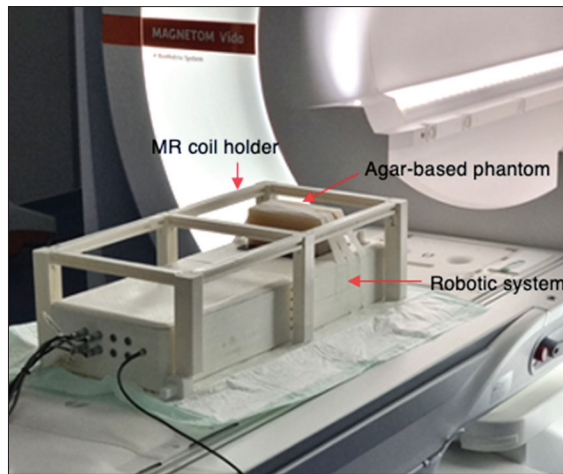


Figure 3: Experimental setup with the robotic system accommodated on the table of the 3T magnetic resonance imaging scanner and the agar-based phantom positioned on the acoustic opening of the system

TE = 10 ms, FOV: $28 \times 28 \text{ cm}^2$, Slice thickness = 10 mm, Acquisition matrix = 128×128 , NEX = 1, ETL = 1, and Flip angle = 35°) as the FSPGR sequence. Correspondingly, agar-based phantoms received a SAR of 0.6877 W/kg during the FLASH imaging performed inside the 3T MRI scanner.

PRF-based MR thermometry calculations for sonications within the 1.5T and 3T scanners were executed using FSPGR and FLASH images acquired in both coronal and axial planes, that were respectively loaded into the developed MRgFUS control and MR monitoring software. For both field strengths (1.5T and 3T) and imaging planes (coronal and axial), the time series temperature plots and color-coded thermal maps as overlaid on the corresponding magnitude images of the agar-based phantom were extracted from the software.

MAGNETIC RESONANCE THERMOMETRY FOR SONICATIONS AT 3T

Signal-to-noise ratio dependence and magnetic resonance thermometry sensitivity with varied TE values

A series of equivalent sonications were executed on the agar-based phantom that was scanned in the coronal plane using the FLASH pulse sequence with the abovementioned acquisition parameters. Regarding the TE value of the FLASH sequence, scans were performed with varied TE values of 5, 10, 15, and 20 ms to assess the effect of the TE on the SNR of the acquired images, and ultimately the effect on the temperature changes measured with PRF MR thermometry.

For each FLASH image acquired with a varied TE value, SNR estimations were implemented by measuring the average signal intensity of the image in two specific ROIs set inside the agar-based phantom and the air background, respectively, and using the following equation:

$$SNR = \frac{SI_{phantom}}{\sigma_{noise}} \quad (2)$$

where $SI_{phantom}$ represents the average signal intensity of the

ROI set within the agar-based phantom, while σ_{noise} indicates the standard deviation of the signal intensity measurements of the ROI set in the air background. Noteworthy, noise in the air background was assumed to follow a Gaussian distribution.

Magnetic resonance thermometry for sonications on agar-based phantoms with varied inclusions

MR thermometry data were generated for monitoring single sonications executed on three agar-based phantoms developed with different compositions of the three inclusion materials (agar, silica, and evaporated milk). For development of the three phantoms, the composition of agar remained constant at 6% w/v with the % composition of additional inclusions varying. In this regard, a 6% w/v agar phantom, a 6% w/v agar, 2% w/v silica phantom, and a 6% w/v agar, 2% w/v silica, 30% v/v evaporated milk phantom were developed and used as sonication targets. It is worth mentioning that the three phantoms were developed in a manner that enabled their simultaneous accommodation on the acoustic opening of the system.

RESULTS

Magnetic resonance thermometry for sonications at 1.5T and 3T

PRF-based MR thermometry was performed for identical sonication protocols (acoustic power of 60 W for 60 s at a focal depth of 40 mm) executed on an agar-based phantom (6% w/v agar) inside the two MRI scanners of different magnetic field strength. MR thermometry for the single sonications executed within the 1.5T MRI scanner (Signa HDxt 16x, GE Healthcare) generated thermal maps with a temporal resolution of 6.6 s using the FSPGR sequence. Accordingly, sonications performed on the same agar-based phantom (6% w/v agar) using an identical ultrasonic protocol (acoustic power of 60 W for 60 s) within the 3T MRI scanner (Magnetom Vida, Siemens Healthineers) and imaged with a FLASH sequence with identical acquisition parameters as the corresponding FSPGR sequence at 1.5T, resulted in thermal maps generated in time intervals of 2.6 s during sonications. Figure 4a and b show the coronal thermal maps of the agar-based phantom produced at specific times throughout sonications implemented within the 1.5T and 3T scanners, respectively. The evolution of heating during sonications is observed at specific ROIs within the agar-based phantom through the overlay of the colour-coded thermal map on the respective magnitude image of the agar-based phantom as acquired at either of the two MRI scanners of varied magnetic field strength.

Regarding sonications executed at the higher field scanner (3T), maximum temperatures (T10 percentile) of 47.8°C were recorded within the agar-based phantom at the focus, in a plane perpendicular to the beam (coronal plane) as shown in the temperature evolution timeseries graph in Figure 5. Figure 6a and b show the thermal maps produced in an axial plane (parallel

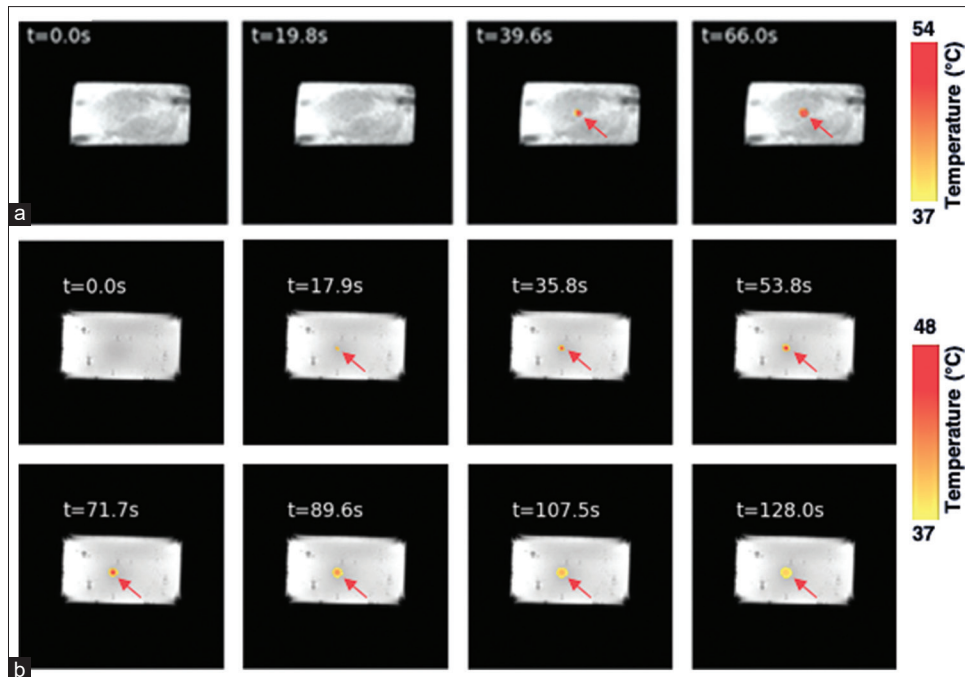


Figure 4: Coronal thermal maps of the agar-based phantom obtained during sonications with a 2.6 MHz transducer at acoustic power of 60 W for a sonication time of 60 s at 40 mm focal depth. Colour-coded temperature increase observed at the focal spot within the phantom (red arrows) at different timepoints for sonications inside (a) a 1.5T scanner, and (b) a 3T scanner

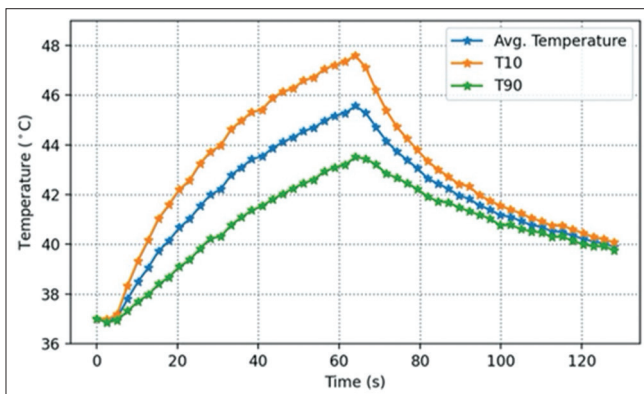


Figure 5: Temperature evolution observed within the agar-based phantom in coronal plane during sonications with a 2.6 MHz transducer at acoustic power of 60 W for a sonication time of 60 s at 40 mm focal depth inside a 3T scanner

to the ultrasonic beam propagation) at different timepoints during sonications, as generated with MR thermometry for equivalent sonications (acoustic power of 60 W for 60 s) at 1.5T and 3T, respectively. Correspondingly, the advancement of thermal heating during exposure, as well as the diffusion of heating after the elapsed sonication time are noticeable within the agar-based phantom at both 1.5T and 3T scanners.

Magnetic resonance thermometry at 3T

Magnetic resonance thermometry for assessing effect of acoustic power on temperature change

MR images acquired during single sonications performed on a 6% w/v agar, 2% w/v silica phantom utilizing varied acoustic

power (1.5, 3, 6, 9, 15, 30, and 45 W) for a constant sonication time of 60 s at equivalent focal depths (45 mm) were processed with MR thermometry to assess the effect of the varied acoustic power on the MR thermometry calculated temperature change. Figure 7a shows the maximum temperature change, from a baseline of 37°C, induced resulting application of varied acoustic power (1.5, 3, 6, 9, 15, 30, and 45 W). Following linear regression ($R^2 = 0.9811$), a proportional dependency between the induced temperature change and the applied acoustic power was discovered as shown in Figure 7a. Accordingly, Figure 7b shows thermal maps acquired at different timepoints during sonications executed at an acoustical power of 1.5 W. Thermal heating at the focal spot was clearly visible on the thermal maps as shown in Figure 7b.

Signal-to-noise ratio dependence and magnetic resonance thermometry sensitivity with varied echo time values

Figure 8a shows a bar chart of the SNR calculated from FLASH images acquired with varied TE values (5, 10, 15, and 20 ms) during sonications executed on the agar-based phantom doped with silica (6% w/v agar, 2% w/v silica) using a constant sonication protocol (acoustic power of 45 W for a sonication time of 30 s at a focal depth of 35 mm). In general, a decreased SNR was observed with increased TE values. Accordingly, Figure 8b shows the effect of the varied TE (5, 10, 15, and 20 ms) used for imaging on the temperature changes (from a baseline temperature of 37°C) measured with MR thermometry in the coronal plane (perpendicular to the ultrasonic beam).

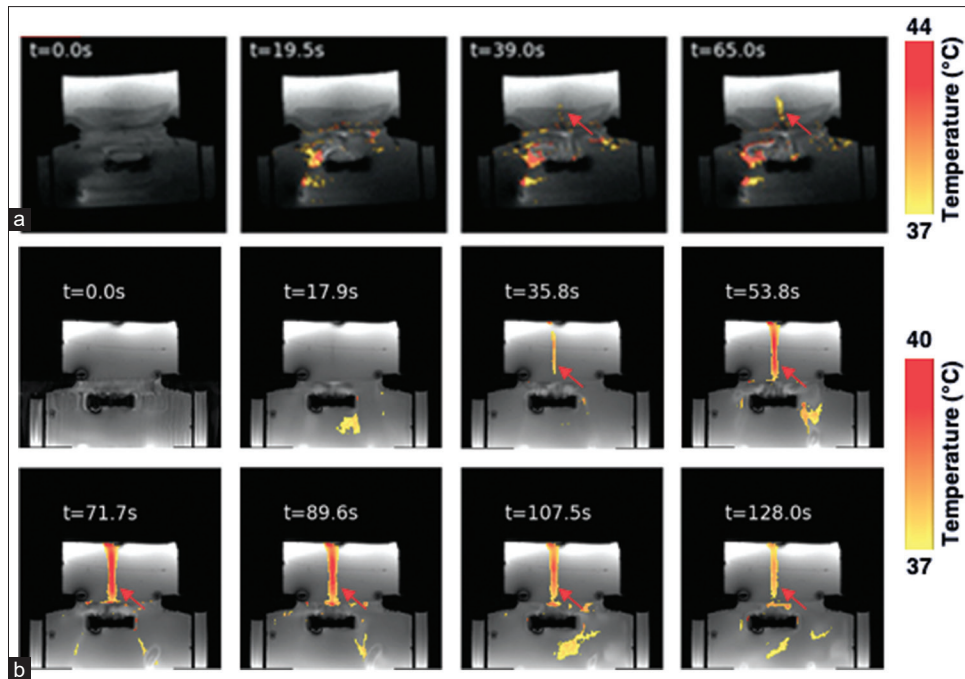


Figure 6: Axial thermal maps of the agar-based phantom obtained during sonications with a 2.6 MHz transducer at acoustic power of 60 W for a sonication time of 60 s at 40 mm focal depth. Color-coded temperature increase observed at the focal spot within the phantom (red arrows) at different timepoints for sonications inside (a) a 1.5T scanner, and (b) a 3T scanner

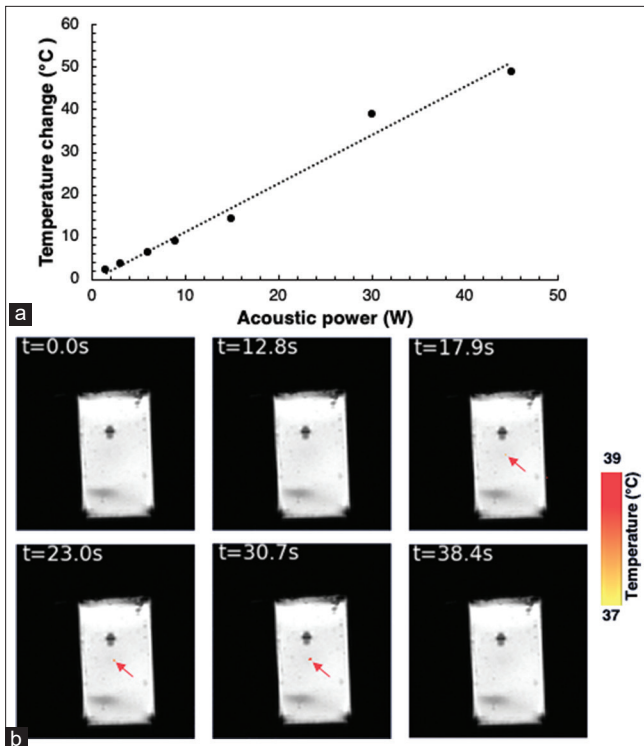


Figure 7: (a) Temperature changes observed within an agar-based phantom for sonications executed at varied acoustic power (1.5 W, 3 W, 6 W, 9 W, 15 W, 30 W, 45 W) for a constant sonication time of 60 s using the 2.6 MHz transducer at a focal depth of 45 mm inside a 3T scanner, and (b) Coronal thermal maps of the agar-based phantom obtained at different timepoints during sonications at the acoustic power of 1.5 W showing thermal heating at the focal spot (red arrows)

Magnetic resonance thermometry for sonications on agar-based phantoms with varied inclusions

Thermal maps were generated at specific time intervals for identical sonications (acoustic power of 45 W for sonication time of 60 s at a focal depth of 45 mm) that were implemented on the three agar-based phantoms having varied inclusions. Thermal maps generated in a coronal plane are indicatively shown in Figure 9a at different timepoints during sonications performed on the agar-based phantom doped with silicon dioxide (6% w/v agar, 2% w/v silica), showing the amount of thermal heating gradually induced at the focal spot within the phantom. The acoustic power of 45 W applied for a sonication time of 60 s on the 6% w/v agar, 2% w/v silica phantom was sufficient to induce T90 percentile, average, and T10 percentile temperatures of 70°C, 79°C and 86°C, respectively, as shown in the time series temperature graph of the sonications in Figure 9b. Correspondingly, temperatures induced on the remaining two agar-based phantoms resulting analogous sonications, were sufficiently high as shown in Table 1. The maximum temperatures (T10 percentile) for the three phantoms induced by application of the constant ultrasonic protocol ranged between 78°C and 87°C, therefore indicating maximum temperature changes between 41°C and 50°C from the baseline temperature of 37°C.

Magnetic resonance thermometry for grid sonications on an agar-based phantom

The FLASH images acquired in a coronal plane during sonications (acoustic power of 60 W for a sonication time of 60 s at a 45 mm focal depth) executed in a 3 × 3 grid with a 10 mm spatial step on the agar-based phantom (6% w/v agar,

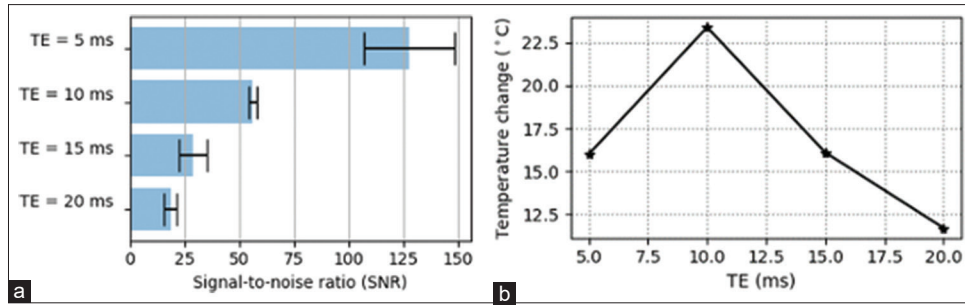


Figure 8: (a) Bar chart of signal-to-noise ratio for four fast low angle shot scans acquired with different echo time (TE) values. The error bars indicate standard error across images within a scan, and (b) Maximum temperature change measured in coronal plane for different TE values resulting sonications executed on the agar-based phantom using the 2.6 MHz transducer at acoustic power of 45 W for a sonication time of 30 s at 35 mm focal depth inside a 3T scanner

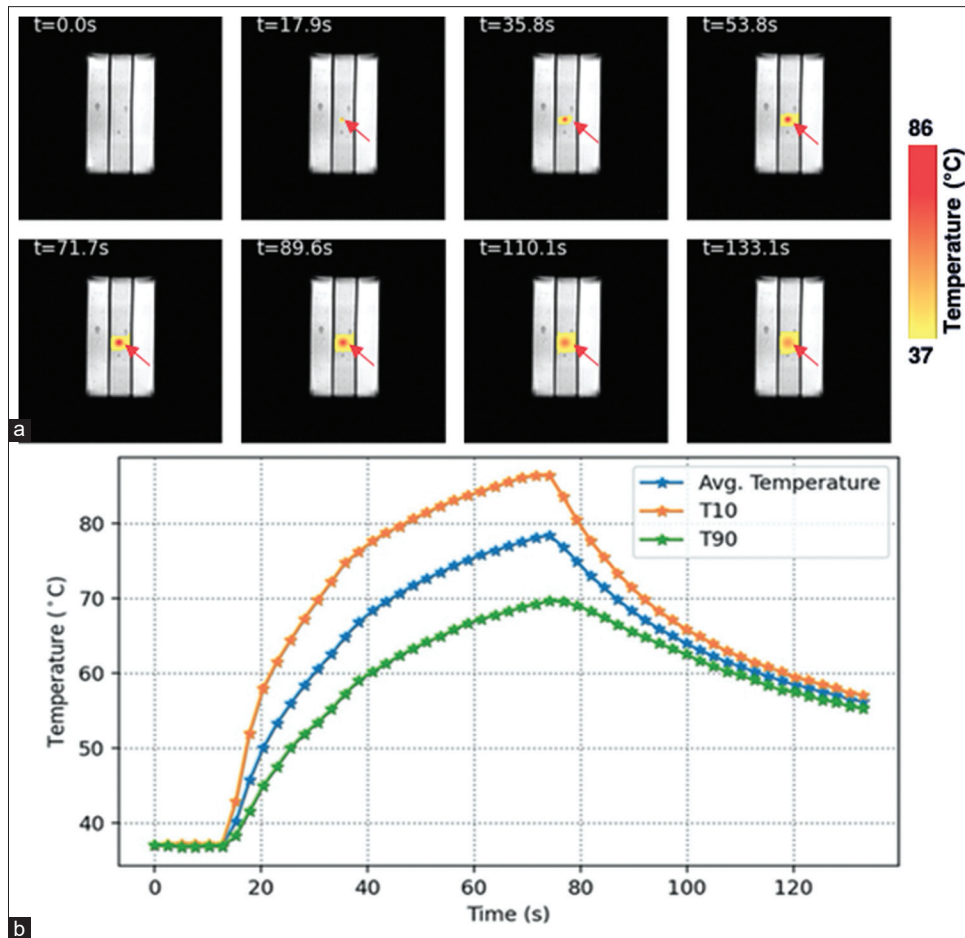


Figure 9: (a) Coronal thermal maps of the agar-based phantom (6% w/v agar, 2% w/v silica) acquired at different timepoints during sonications with a 2.6 MHz transducer at acoustic power of 45 W for a sonication time of 60 s at 45 mm focal depth inside a 3T scanner showing thermal heating at the focal spot (red arrows), and (b) Time series temperature graph of the sonications

2% w/v silica), provided real-time monitoring of the location of the thermal heating at each of the nine sonication points of the specified grid as shown in Figure 10. The accumulation of thermal heating at each sonication point was visualized as a small black spot on the acquired magnitude images presented for each of the nine sonications at approximately the end of each sonication time (60 s).

Accordingly, MR thermometry for the grid sonications executed on the 6% w/v agar, 2% w/v silica phantom,

produced sufficiently rapid thermal maps, resulting in a 2.6 s temporal resolution. Figure 11 shows the coronal thermal maps generated for each of the nine sonication points of the specified grid operation at roughly toward the end of each 60 s sonication time (limited by the temporal resolution). Overlap of the thermal maps on the magnitude images of the agar-based phantom clearly indicates increased thermal heating accumulated at the respective grid sonication point and shows the extent of the diffusion of thermal heating throughout the

Table 1: Temperature change recorded within three different agar-based phantoms during sonications with a 2.6 MHz transducer at acoustic power of 45 W for a sonication time of 60 s at 45 mm focal depth inside a 3T scanner

Phantom	Maximum temperature (°C)	Maximum ΔT (°C)
6% w/v agar	78	41
6% w/v agar, 2% w/v silica	86	49
6% w/v agar, 2% w/v silica, 30% v/v milk	87	50

w/v: Weight per volume, v/v: Volume per volume, ΔT : Temperature changes

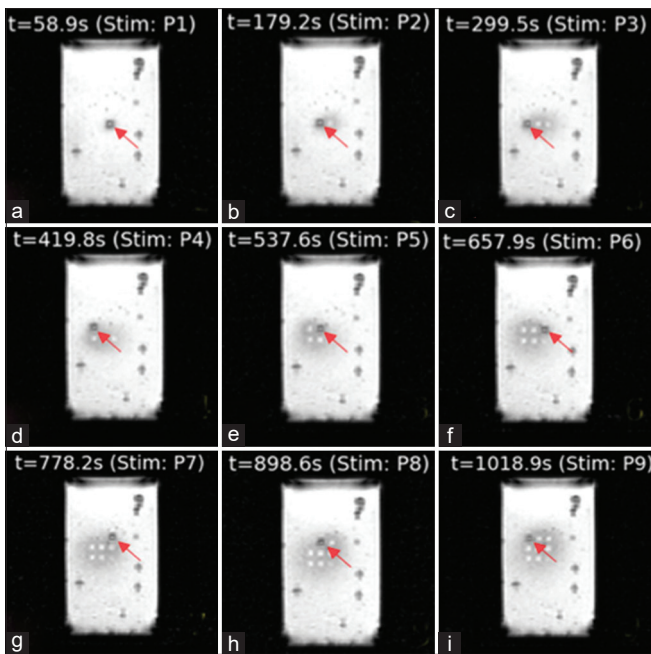


Figure 10: Coronal magnitude images of the agar-based phantom obtained during a series of sonications with a 2.6 MHz transducer in a 3×3 grid (10 mm distance between successive points) using an acoustic power of 45 W for a sonication time of 60 s at 45 mm focal depth inside a 3T scanner. Red arrows indicate thermal heating. Images acquired at the end of sonications at (a) 1st grid point, (b) 2nd grid point, (c) 3rd grid point, (d) 4th grid point, (e) 5th grid point, (f) 6th grid point, (g) 7th grid point, (h) 8th grid point, and (i) 9th grid point

agar-based phantom as well as the heating remaining from previous sonications.

DISCUSSION

In the present study, the sensitivity of MR thermometry based on the extensively employed PRF technique,^[5,6] was assessed for a series of HIFU sonications executed on agar-based phantoms within a clinical 3T MRI scanner. Some sonications were also executed within a 1.5T MRI, to assess the sensitivity and quality of the MR thermometry temperature mapping in the lower field clinical scanner. Notably, HIFU sonications were performed using a previously developed preclinical MRgFUS

robotic system^[43] equipped with a 2.6 MHz single element focused transducer, and controlled with an inhouse developed MRgFUS software that enables temperature monitoring through PRF-based MR thermometry tools.^[47]

Initially, comparable sonications were executed on an agar-based phantom within the two clinical MRI scanners of varied magnetic field strength to assess the performance of the system and compare MR thermometry-based temperature mapping between the two scanners. Although the two scanners were from different vendors and some differences between scanner parameters, other than field strength, existed (i.e., maximum gradient amplitude, homogeneity, and slew rate), the effect of these parameters on the generated PRF thermal mapping was not investigated herein. The quality of MR thermometry mapping was rather investigated based solely on magnetic field strength differences, with the impact of other MRI hardware parameters possibly explored in future studies. MR thermometry was efficiently employed for temperature monitoring, generating color-coded thermal maps during ultrasonic exposures. Notably, thermal maps generated at 1.5T had a 2.5-fold lower temporal resolution (6.6 s) compared to the results at 3T (2.6 s) despite employment of similar imaging sequences with comparable acquisition parameters (NEX was increased by one unit at 1.5T). Furthermore, the thermal maps generated at the higher magnetic field strength scanner (3T), were characterized by an increased image quality with decreased artifacts (presence of grey shadows within the agar-based phantom) compared to the corresponding maps produced at 1.5T. Nevertheless, despite inherent similarities between the two imaging sequences, the ultrafast gradient echo sequence that was utilized at 1.5T differs in the sense that a 180° inversion pulse is initially utilized before data acquisition, while the spoiled gradient echo sequence that was employed at the 3T scanner applies a spoiler gradient prior to acquisition of new data, thus minimizing remaining transverse magnetization and reducing image artifacts.^[55] In addition, the FSPGR sequence employed at 1.5T induced a higher SAR within the agar-based phantoms compared to the FLASH sequence utilized for imaging at the 3T scanner, indicating approximately a 2.5-fold increased electromagnetic energy absorbed by phantoms during imaging at the lower field strength MRI scanner. Nevertheless, at both MRI scanners sufficiently high temperatures were recorded with MR thermometry, thus indicating the efficacy of the monitoring method and the accuracy of the calculations.

On validating that MR thermometry at 3T results in higher quality thermal mapping, a series of sonications were exclusively executed within the higher magnetic field clinical scanner to assess the effect of various experimental parameters (sonication target, sonication parameters, or image acquisition parameters) on the MR thermometry temperature measurements. In this regard, the effect of applied acoustic power on the temperature change was initially examined for a series of sonications of constant exposure, wherein by linear regression, a proportional relationship was observed.

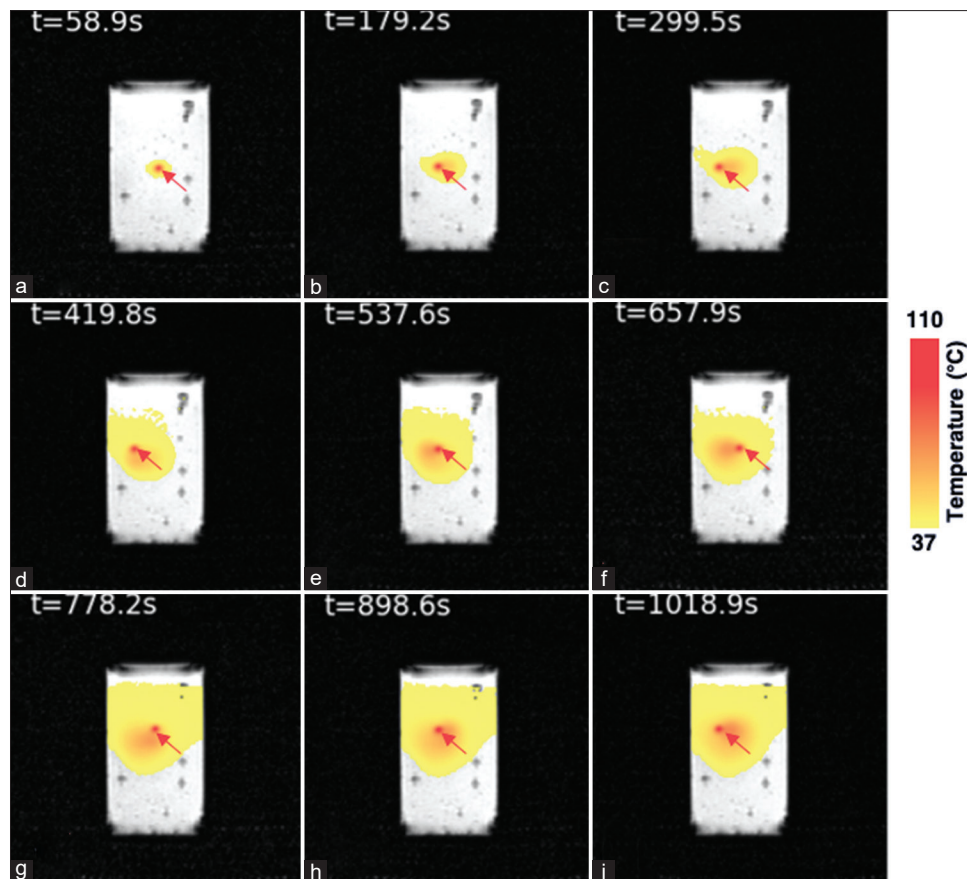


Figure 11: Coronal thermal maps of an agar-based phantom acquired during sonications with a 2.6 MHz transducer in a 3×3 grid with a 10 mm step using an acoustic power of 45 W for a sonication time of 60 s at 45 mm focal depth inside a 3T scanner showing thermal heating at focal spot (red arrows). Maps acquired at the end of sonications at (a) 1st grid point, (b) 2nd grid point, (c) 3rd grid point, (d) 4th grid point, (e) 5th grid point, (f) 6th grid point, (g) 7th grid point, (h) 8th grid point, and (i) 9th grid point

Particularly, temperature changes in the range of 2.3°C – 49°C were recorded for varied applied acoustic power between 1.5 and 45 W, resulting in a 1.14 increase in temperature change for a unit increase in the applied acoustic power. Furthermore, acquired thermal maps indicated that thermal heating within the agar-based phantom was detectable at the lowest applied acoustic power of 1.5 W, thus providing insights on the lowest acoustic power that can provide reliable detection of the ultrasonic beam within a single image voxel with volume of $2.18 \text{ mm} \times 2.18 \text{ mm} \times 10 \text{ mm}$. It is worth stating that the lowest acoustic power for optimal beam detection as established herein, is only valid for the current sonication target and transducer, since heat transfer at the focal spot is dependent on several tissue parameters, the mode of the exposure, and the structural characteristics of the focused transducer.^[2] Although the proposed acoustic power is conservative in this regard, current values could be potentially used in preclinical MRgFUS studies executed on agar-based phantoms using transducers of similar characteristics, to provide reliable visualization of the beam on MR imaging during sonications that induce temperature increases below permanent damage thresholds.

More importantly, the effect of the scanning parameters of the FLASH imaging sequence, specifically the TE, on the

SNR of the magnitude images and the thermometry-based temperature measurements was successfully assessed. Standard SNR calculations performed for a series of MR images acquired during identical ultrasonic exposures using varied TE values in the range of 5–20 ms (5 ms step) revealed a negative effect of the increased TE on the image SNR and therefore on image quality. Specifically, a TE of 5 ms exhibited an SNR of 127.7 ± 20.8 that decreased by almost 85% to an SNR value of 18.4 ± 3.1 for a 4-fold increase in the TE (20 ms). Appropriately, for the varied TE values examined temperature changes between 12°C and 23°C were recorded, with the highest temperature change measured at the TE of 10 ms. Notably, for a TE at 5 ms, temperature changes of 16°C were recorded, despite this TE value exhibiting the highest image quality in terms of SNR. Contrary, the TE of 20 ms resulted in a temperature change of only 12°C , in accordance to presenting with the lowest SNR and the most inferior image quality. The increased spatial resolution of MR thermometry-based temperature measurements observed with higher TE values in the present study, is consistent with similar temperature resolution dependencies reported with the acquisition parameters for other types of sequences (EPI) during MRgFUS sonications at 3T.^[28] Nevertheless, although

SNR calculations in the present study were executed using a standard approach, the employed method has been reported to result in significantly inaccurate SNR calculations.^[56] In this manner, retrospective SNR calculations executed in this study for images acquired at varied TE values might be over or underestimated by approximately 34%.^[56] However, since background noise was homogeneously distributed in images acquired at varied TE values, similar inaccuracies in the calculated SNR values for each TE value would be expected, thus still making inherent the effect of varying TE on the SNR of magnitude FLASH images.

Moreover, the effect of the varied inclusion materials employed for development of three agar-based phantoms on the MR thermometry measurements was examined. Silica and evaporated milk were utilized as additional inclusions since they have previously shown to enhance the scattering^[38] and absorption^[57] properties of the developed phantoms, respectively. Application of a constant ultrasonic protocol on the three phantoms sufficiently induced high temperature increases. Inherently, addition of silica in a 2% w/v concentration exhibited approximately 20% higher temperature increases (49°C–50°C) compared to the purely agar-based phantom (6% w/v) (41°C). These findings suggest that addition of silica enhances the absorption of acoustic energy, resulting in higher temperatures for identical ultrasonic protocols compared to phantoms developed merely with agar, which do not seem to absorb a notable amount of ultrasonic energy. That said, Menikou *et al.*^[41] demonstrated that addition of silica in agar-based phantoms introduces absorption-based ultrasonic attenuation mechanisms that are reflected in the increased temperatures recorded within these phantoms during ultrasonic exposures. In this context, results presented herein, replicate the findings previously presented by Menikou *et al.*,^[41] thus further validating the accuracy of the MR thermometry calculations performed herein.

Sonifications executed in a grid manner confirmed the accurate navigation of the transducer in predetermined trajectories, evidenced by the equally spaced thermal heating spots that were visualized on the magnitude FLASH images of the agar-based phantom acquired during exposures. Moreover, generated thermal maps, indicated that temperatures close to 100°C were consistently produced resulting sonifications at each of the grid sonication points. Nevertheless, thermal maps revealed that thermal heating at each of the sonication points remained until subsequent sonifications, thus contributing to the overall accumulation of thermal heating within the targeted trajectory during exposures. As a result, the high temperatures that were consistently produced, were sufficient to create demarcated circular lesions (visualized as white spots) at each of the nine sonication points, indicating that the temperatures induced by sonifications surpassed the temperature threshold of the melting point of agar.^[58]

Overall, successful MR thermometry monitoring, using an inhouse developed software,^[44] was achieved in the present

study for HIFU sonifications performed within a clinical 3T scanner, with the MR thermometry data generated with a short temporal resolution (~2.6 s). However, the temporal resolution could be further enhanced in future experiments through employment of EPI sequences that are known to result in more rapid imaging and thermal mapping.^[8,10] Moreover, while thermometry data indicated successful performance of the MRgFUS system within both MRI environments, increased quality of acquired images was observed at 3T compared to similar sonifications performed at 1.5T. Future studies could quantitatively examine differences in the MR thermometry temperature accuracy between the two varied magnetic field strengths to determine whether higher accuracies are achieved at the higher field scanner for the sequences and experimental settings employed in the present study, as previously demonstrated in the literature for other types of sequences and MRgFUS systems.^[8] In this sense, associations between image quality and temperature measurement accuracies between the two varied field strength scanners could be derived. Moreover, the FLASH sequence employed herein for MR image acquisition, was optimized in terms of TE for optimal SNR and temperature sensitivity. Nevertheless, considering that optimal SNR is often achieved when the TE is in the same range as the T2* relaxation times of the tissue under investigation,^[14] and given that T2* relaxation times of these agar-based phantoms were recently measured between 18.5 and 21.7 ms at 3T,^[59] a TE of 10 ms was considered optimal herein to achieve sufficiently high image quality. Consequently, although image acquisition parameters are well optimized for clinical PRF MR thermometry,^[14] results presented herein are conservative in the sense that they are optimized for the employed experimental setup. Nevertheless, acquisition parameters as suggested in this study could be proven useful for MR thermometry during future preclinical MRgFUS studies executed on agar-based phantoms, reducing time needed for optimization of the thermometry sequence. Moreover, insightful observations were derived relating to the dependency of the spatial resolution of temperature with the HIFU sonication parameters (acoustic power) and the inclusions of the agar-based phantoms. Results presented herein demonstrated the sensitivity, spatial and temporal resolution of MR thermometry monitoring using the PRF technique at 3T for HIFU sonifications on agar-based phantoms. Present data could be used in future preclinical MRgFUS feasibility studies executed on agar-based phantoms to enhance MR thermometry techniques for optimal monitoring and evaluation of novel MRgFUS systems.

Acknowledgments

The authors would like to express their gratitude to Samuel Pichardo (Cumming School of Medicine, University of Calgary, Calgary, Alberta, Canada) for providing the Python libraries (Proteus MRI-HIFU Software Development Suite) for MR thermometry calculations.

Financial support and sponsorship

The study has been co-funded by the European Structural and Investment Funds and the Republic of Cyprus through

the Research and Innovation Foundation under the projects SOUNDPET (INTEGRATED/0918/0008).

Conflicts of interest

There are no conflicts of interest.

REFERENCES

- Fry WJ, Mosberg WH Jr., Barnard JW, Fry FJ. Production of focal destructive lesions in the central nervous system with ultrasound. *J Neurosurg* 1954;11:471-8.
- Ter Haar G. HIFU tissue ablation: Concept and devices. In: Escoffre JM, A Bouakaz A, editors. *Advances in Experimental Medicine and Biology*. Vol. 880. Cham: Springer; 2016. p. 3-20.
- Siedek F, Yeo SY, Heijman E, Grinstein O, Bratke G, Heneweer C, *et al.* Magnetic resonance-guided high-intensity focused ultrasound (MR-HIFU): Technical background and overview of current clinical applications (Part 1). *RöFo - Advances in the field of X-rays and medical imaging* 2019;191:522-30.
- González-Hernando C, Esteban L, Cañas T, Van den Brule E, Pastrana M. The role of magnetic resonance imaging in oncology. *Clin Transl Oncol* 2010;12:606-13.
- Rieke V, Pauly KB. MR thermometry. *J Magn Reson Imaging* 2008;27:376-90.
- Odéen H, Parker DL. Magnetic resonance thermometry and its biological applications – Physical principles and practical considerations. *Prog Nucl Magn Reson Spectrosc* 2019;110:34-61.
- Kuroda K. MR techniques for guiding high-intensity focused ultrasound (HIFU) treatments. *J Magn Reson Imaging* 2018;47:316-31.
- Kickhefel A, Roland J, Weiss C, Schick F. Accuracy of real-time MR temperature mapping in the brain: A comparison of fast sequences. *Phys Med* 2010;26:192-201.
- Wang P. Evaluation of MR thermometry with proton resonance frequency method at 7T. *Quant Imaging Med Surg* 2017;7:259-66.
- Weidensteiner C, Quesson B, Caire-Gana B, Keroui N, Rullier A, Trillaud H, *et al.* Real-time MR temperature mapping of rabbit liver *in vivo* during thermal ablation. *Magn Reson Med* 2003;50:322-30.
- Stafford RJ, Price RE, Diederich CJ, Kangasniemi M, Olsson LE, Hazle JD. Interleaved echo-planar imaging for fast multiplanar magnetic resonance temperature imaging of ultrasound thermal ablation therapy. *J Magn Reson Imaging* 2004;20:706-14.
- Yuan J, Mei CS, Panych LP, McDannold NJ, Madore B. Towards fast and accurate temperature mapping with proton resonance frequency-based MR thermometry. *Quant Imaging Med Surg* 2012;2:21-32.
- Marx M, Plata J, Pauly KB. Toward volumetric MR thermometry with the MASTER sequence. *IEEE Trans Med Imaging* 2015;34:148-55.
- Chung AH, Hynynen K, Colucci V, Oshio K, Cline HE, Jolesz FA. Optimization of spoiled gradient-echo phase imaging for *in vivo* localization of a focused ultrasound beam. *Magn Reson Med* 1996;36:745-52.
- Marx M, Butts Pauly K. Improved MRI thermometry with multiple-echo spirals. *Magn Reson Med* 2016;76:747-56.
- O'Neill BE, Karmonik C, Sassaroli E, Li KC. Estimation of thermal dose from MR thermometry during application of nonablative pulsed high intensity focused ultrasound. *J Magn Reson Imaging* 2012;35:1169-78.
- Bing C, Staruch RM, Tillander M, Köhler MO, Mougnot C, Yliahautala M, *et al.* Drift correction for accurate PRF-shift MR thermometry during mild hyperthermia treatments with MR-HIFU. *Int J Hyperthermia* 2016;32:673-87.
- Ozhinsky E, Salgaonkar VA, Diederich CJ, Rieke V. MR thermometry-guided ultrasound hyperthermia of user-defined regions using the exablate prostate ablation array. *J Ther Ultrasound* 2018;6:7.
- Hijnen NM, Elevelt A, Pikkemaat J, Bos C, Bartels LW, Grüll H. The magnetic susceptibility effect of gadolinium-based contrast agents on PRFS-based MR thermometry during thermal interventions. *J Ther Ultrasound* 2013;1:8.
- Schmitt A, Mougnot C, Chopra R. Spatiotemporal filtering of MR-temperature artifacts arising from bowel motion during transurethral MR-HIFU. *Med Phys* 2014;41:113302.
- Pichardo S, Köhler M, Lee J, Hynynen K. *In vivo* optimisation study for multi-baseline MR-based thermometry in the context of hyperthermia using MR-guided high intensity focused ultrasound for head and neck applications. *Int J Hyperthermia* 2014;30:579-92.
- Salomir R, Viallon M, Kickhefel A, Roland J, Morel DR, Petrusca L, *et al.* Reference-free PRFS MR-thermometry using near-harmonic 2-D reconstruction of the background phase. *IEEE Trans Med Imaging* 2012;31:287-301.
- Holbrook AB, Santos JM, Kaye E, Rieke V, Pauly KB. Real-time MR thermometry for monitoring HIFU ablations of the liver. *Magn Reson Med* 2010;63:365-73.
- Ferrer CJ, Bartels LW, van der Velden TA, Grüll H, Heijman E, Moonen CT, *et al.* Field drift correction of proton resonance frequency shift temperature mapping with multichannel fast alternating nonselective free induction decay readouts. *Magn Reson Med* 2020;83:962-73.
- Rieke V. MR thermometry. In: Kahn T, Busse H, editors *Interventional Magnetic Resonance Imaging*. Berlin, Heidelberg: Springer; 2011. p. 271-88.
- Hindman JC. Proton resonance shift of water in the gas and liquid states. *J Chem Phys* 1966;44:4582-92.
- de Zwart JA, Vimeux FC, Delalande C, Canioni P, Moonen CT. Fast lipid-suppressed MR temperature mapping with echo-shifted gradient-echo imaging and spectral-spatial excitation. *Magn Reson Med* 1999;42:53-9.
- Ramsay E, Mougnot C, Köhler M, Bronskill M, Klotz L, Haider MA, *et al.* MR thermometry in the human prostate gland at 3.0T for transurethral ultrasound therapy. *J Magn Reson Imaging* 2013;38:1564-71.
- Baron P, Deckers R, de Greef M, Merckel LG, Bakker CJ, Bouwman JG, *et al.* Correction of proton resonance frequency shift MR-thermometry errors caused by heat-induced magnetic susceptibility changes during high intensity focused ultrasound ablations in tissues containing fat. *Magn Reson Med* 2014;72:1580-9.
- Baron P, Deckers R, Bouwman JG, Bakker CJ, de Greef M, Viergever MA, *et al.* Influence of water and fat heterogeneity on fat-referenced MR thermometry. *Magn Reson Med* 2016;75:1187-97.
- Diakite M, Odéen H, Todd N, Payne A, Parker DL. Toward real-time temperature monitoring in fat and aqueous tissue during magnetic resonance-guided high-intensity focused ultrasound using a three-dimensional proton resonance frequency T1 method. *Magn Reson Med* 2014;72:178-87.
- Chavez S, Xiang QS, An L. Understanding phase maps in MRI: A new outline phase unwrapping method. *IEEE Trans Med Imaging* 2002;21:966-77.
- Domínguez-Guzmán G, Castillo-Mixcóatl J, Beltrán-Pérez G, Muñoz-Aguirre S. Itoh algorithm to unwrap 2D phase. In: *Proceedings of the Seventh Symposium Optics in Industry*. Guadalajara, Jalisco, Mexico: Society of Photo-Optical Instrumentation Engineers (SPIE); 2009;7499.
- Itoh K. Analysis of the phase unwrapping algorithm. *Appl Opt* 1982;21:2470.
- Herráez MA, Burton DR, Lalor MJ, Gdeisat MA. Fast two-dimensional phase-unwrapping algorithm based on sorting by reliability following a noncontinuous path. *Appl Opt* 2002;41:7437-44.
- Kim EJ, Jeong K, Oh SJ, Kim D, Park EH, Lee YH, *et al.* MR thermometry analysis program for laser-or high-intensity focused ultrasound (HIFU)-induced heating at a clinical MR scanner. *J Korean Phys Soc* 2014;65:2126-31.
- Yiallouras C, Damianou C. Review of MRI positioning devices for guiding focused ultrasound systems. *Int J Med Robot Comput Assist Surg* 2015;11:247-55.
- Drakos T, Antoniou A, Evripidou N, Alecou T, Giannakou M, Menikou G, *et al.* Ultrasonic attenuation of an agar, silicon dioxide, and evaporated milk gel phantom. *J Med Ultrasound* 2021;29:239-49.
- Antoniou A, Georgiou L, Christodoulou T, Panayiotou N, Ioannides C, Zamboglou N, *et al.* MR relaxation times of agar-based tissue-mimicking phantoms. *J Appl Clin Med Phys* 2022;23:e13533.
- Menikou G, Yiannakou M, Yiallouras C, Ioannides C, Damianou C. MRI-compatible breast/rib phantom for evaluating ultrasonic thermal exposures. *Int J Med Robot Comput Assist Surg* 2018;14:e1849.
- Menikou G, Dadakova T, Pavlina M, Bock M, Damianou C. MRI compatible

- head phantom for ultrasound surgery. *Ultrasonics* 2015;57:144-52.
42. Menikou G, Damianou C. Acoustic and thermal characterization of agar based phantoms used for evaluating focused ultrasound exposures. *J Ther Ultrasound* 2017;5:14.
 43. Giannakou M, Antoniou A, Damianou C. Preclinical robotic device for magnetic resonance imaging guided focussed ultrasound. *Int J Med Robot Comput Assist Surg* 2023;19:e2466.
 44. Peters RD, Hinks RS, Henkelman RM. *Ex vivo* tissue-type independence in proton-resonance frequency shift MR thermometry. *Magn Reson Med* 1998;40:454-9.
 45. Botnar RM, Steiner P, Dubno B, Erhart P, von Schulthess GK, Debatin JF. Temperature quantification using the proton frequency shift technique: *In vitro* and *in vivo* validation in an open 0.5 tesla interventional MR scanner during RF ablation. *J Magn Reson Imaging* 2001;13:437-44.
 46. Peters RD, Chan E, Trachtenberg J, Jothy S, Kapusta L, Kucharczyk W, *et al.* Magnetic resonance thermometry for predicting thermal damage: An application of interstitial laser coagulation in an *in vivo* canine prostate model. *Magn Reson Med* 2000;44:873-83.
 47. Filippou A, Georgiou A, Nikolaou A, Evripidou N, Damianou C. Advanced software for MRgFUS treatment planning. *Comput Methods Programs Biomed* 2023;240:107726.
 48. Drakos T, Giannakou M, Menikou G, Filippou A, Evripidou N, Spanoudes K, *et al.* MRI-guided focused ultrasound robotic system for preclinical use. *J Vet Med Anim Sci* 2020;4:1049.
 49. Drakos T, Giannakou M, Menikou G, Damianou C. Magnetic resonance imaging-guided focused ultrasound positioning system for preclinical studies in small animals. *J Ultrasound Med* 2021;40:1343-52.
 50. Spanoudes K, Evripidou N, Giannakou M, Drakos T, Menikou G, Damianou C. A high intensity focused ultrasound system for veterinary oncology applications. *J Med Ultrasound* 2021;29:195-202.
 51. Giannakou M, Drakos T, Menikou G, Evripidou N, Filippou A, Spanoudes K, *et al.* Magnetic resonance image-guided focused ultrasound robotic system for transrectal prostate cancer therapy. *Int J Med Robot Comput Assist Surg* 2021;17:e2237.
 52. Antoniou A, Giannakou M, Evripidou N, Stratis S, Pichardo S, Damianou C. Robotic system for top to bottom MRgFUS therapy of multiple cancer types. *Int J Med Robot Comput Assist Surg* 2022;18:e2364.
 53. Giannakou M, Menikou G, Ioannides K, Damianou C. Magnetic resonance-image-guided focused ultrasound robotic system with four computer-controlled axes with endorectal access designed for prostate cancer focal therapy. *Digit Med* 2020;6:32-43.
 54. Antoniou A, Damianou C. MR relaxation properties of tissue-mimicking phantoms. *Ultrasonics* 2022;119:106600.
 55. Wood ML, Silver M, Runge VM. Optimization of spoiler gradients in FLASH MRI. *Magn Reson Imaging* 1987;5:455-63.
 56. Dietrich O, Raya JG, Reeder SB, Reiser MF, Schoenberg SO. Measurement of signal-to-noise ratios in MR images: Influence of multichannel coils, parallel imaging, and reconstruction filters. *J Magn Reson Imaging* 2007;26:375-85.
 57. Drakos T, Giannakou M, Menikou G, Ioannides C, Damianou C. An improved method to estimate ultrasonic absorption in agar-based gel phantom using thermocouples and MR thermometry. *Ultrasonics* 2020;103:106089.
 58. Ortega R, Téllez A, Leija L, Vera A. Measurement of ultrasonic properties of muscle and blood biological phantoms. *Phys Procedia* 2010;3:627-34.
 59. Antoniou A, Evripidou N, Georgiou L, Chrysanthou A, Ioannides C, Damianou C. Tumor phantom model for MRI-guided focused ultrasound ablation studies. *Med Phys* 2023;50:5956-68.